Journal of Materials Research and Technology 30 (2024) 8661–8670

Contents lists available at ScienceDirect

Journal of Materials Research and Technology

journal homepage: www.elsevier.com/locate/jmrt

Microstructure and failure mechanism of Y_2O_3 coating on the W fiber in W_f/W composites during field assisted sintering

C. Chen [a,b,c,*], Y. Chen [a], X. Han [a], K.L. Li [a], S. Wang [a,d,e,**], Y.F. Zhang [a], Y.R. Mao [f], J.W. Coenen [f,g], J. Wang [a,***], L.M. Luo [a,c]

[a] School of Materials Science and Engineering, Hefei University of Technology, Hefei, 230009, China
[b] Intelligent Manufacturing Institute of HFUT, Hefei, 230009, China
[c] Engineering Research Center of High-Performance Copper Alloy Materials and Processing, Ministry of Education, Hefei University of Technology, Hefei, 230009, China
[d] Institute of Industry and Equipment Technology, Hefei University of Technology, Hefei, 230009, China
[e] Anhui Province Key Lab of Aerospace Structural Parts Forming Technology and Equipment, Hefei University of Technology, Hefei, 230009, China
[f] Institut für Energie und Klimaforschung-Plasmaphysik, Forschungszentrum Jülich GmbH, Jülich, 52425, Germany
[g] Departmentof Nuclear Engineering & Engineering Physics, University of Wisconsin -Madison, 53706, Madison, USA

ARTICLE INFO

Handling editor: SN Monteiro

Keywords:
Tungsten fiber-reinforced tungsten matrix composites
Field assisted sintering
Interfacial microstructure
Y_2O_3 coating
Finite element analysis

ABSTRACT

For tungsten fiber-reinforced tungsten matrix (W_f/W) composites, the interfacial microstructure is essential for the improvement of mechanical properties. The Y_2O_3 coating deposited on the W fiber has been applied to modify the interface between the W matrix and W fiber. However, the Y_2O_3 coating on the W fiber is usually fractured and dispersed into the W matrix as large particles after sintering. In this study, the microstructure of the Y_2O_3 coating on the W fiber in W_f/W composites was studied. And the failure mechanism of Y_2O_3 interface during field assisted sintering was investigated through finite element analysis (FEA). The reasons for the fracture of the Y_2O_3 interface can be attributed to the transformation of the Y_2O_3 coating from cubic to face centered cubic (FCC) crystal structure, the large lattice misfit of 49.0% at the interface, the large difference of the elastic modulus and thermal expansion coefficient between W and FCC-Y_2O_3. In order to avoid the fracture of Y_2O_3 interface during sintering, the finite element analysis was used to modify the processing parameters of W_f/W composites, including the sintering temperature, pressure, particle size of W powder and thickness of the Y_2O_3 coating. And the simulation results were consistent with the experimental results.

1. Introduction

Pure tungsten (W) materials usually show brittle due to its high ductile to brittle transition temperature (about 500 K) and recrystallization brittleness, in which recrystallization occurs at temperatures as low as about 1523 K [1]. The brittleness is a major problem for pure W materials applied as plasma-facing materials in future fusion reactors [2]. In order to improve the fracture toughness of pure W materials, W_f/W composites have been developed based on fiber-reinforced ceramic matrix composites, relying on extrinsic toughing mechanisms, such as pull-out of W fibers, the ductile deformation of the W fibers, crack deflection and/or interface de-bonding [3]. For the W_f/W composites, the interfacial microstructure between W fiber and W matrix plays an important role in the mechanical properties. It has been found that the weak interfacial bonding strength is beneficial for extrinsic toughing mechanism or pseudo-ductile fracture behavior in W_f/W composites [4]. However, the bonding strength between the W fiber and W matrix usually is too high to enable debonding, making the W_f/W composites still brittle [4]. Therefore, the modification of interfacial microstructure has been widely investigated to optimizing the bonding strength.

To achieve a suitable interfacial bonding strength between the W fiber and W matrix, various interfacial materials coated on W fibers have been investigated, such as Cu, Mo, C, ZrO_2, Er_2O_3 and Y_2O_3 et al. [3–8]. Compared with other interfacial materials, Y_2O_3 coating has received considerable attention due to its excellent thermal and chemical

* Corresponding author. School of Materials Science and Engineering, Hefei University of Technology, Hefei, 230009, China.
** Corresponding author. School of Materials Science and Engineering, Hefei University of Technology, Hefei, 230009, China.
*** Corresponding author.
E-mail addresses: chench@hfut.edu.cn (C. Chen), swang@hfut.edu.cn (S. Wang), jwang@hfut.edu.cn (J. Wang).

https://doi.org/10.1016/j.jmrt.2024.05.237
Received 1 April 2024; Received in revised form 13 May 2024; Accepted 27 May 2024
Available online 29 May 2024
2238-7854/© 2024 The Authors. Published by Elsevier B.V. This is an open access article under the CC BY-NC license (http://creativecommons.org/licenses/by-nc/4.0/).

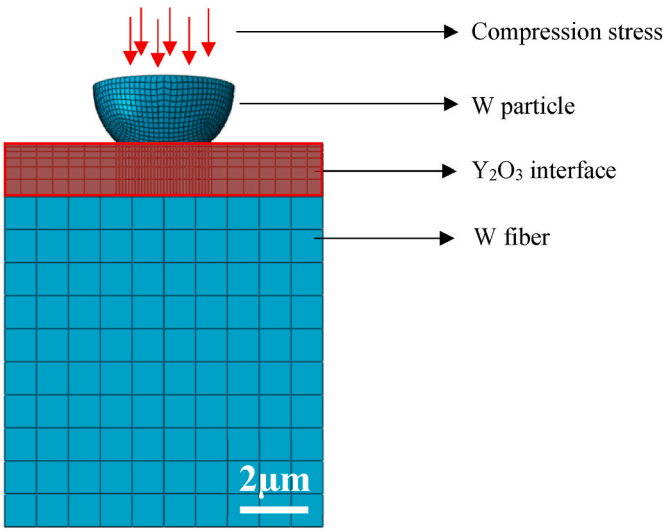

Fig. 1. Geometric diagram of 3D model for FEM analysis.

stability, high mechanical strength and relatively low activation after neuron irradiation [8–10]. The Y_2O_3 coating on the W fiber can improve the fracture toughness of W_f/W composites due to the decrease of interfacial bonding strength between the W matrix and W fiber [4,8]. Meanwhile, the Y_2O_3 interface between the W matrix and W fiber can impede the abnormal recrystallization and grain growth behavior of W fiber in W_f/W composites sintered at temperatures lower than the normal recrystallization temperature of W wires [8].

However, the Y_2O_3 coating was always failure during sintering at high temperatures, which was fractured and dropped from the surface of W fibers as large particles [8–10]. At that condition, the fractured Y_2O_3 coating was bad for the extrinsic toughing mechanism in W_f/W composites. Therefore, several ways have been applied to prevent the fracture of the Y_2O_3 coating, such as increasing the thickness of the Y_2O_3 coating [4], and coating a W layer on the Y_2O_3 coating [10]. However, the results were not so satisfactory since the failure mechanism of Y_2O_3 coating has not been explored. Therefore, the fracture of the Y_2O_3 coating still occurs in W_f/W composites.

In this study, the microstructure of the Y_2O_3 coating on the W fiber in W_f/W composites before and after sintering was investigated. Based on that, the failure mechanism of the Y_2O_3 interface in W_f/W composites during sintering was studied by both experimental investigation and finite element analysis (FEA).

2. The materials and experimental procedures

2.1. The preparation of the Y_2O_3 coating

The short discontinuous W_f/W composites were prepared by powder metallurgy in this study. The original short as-drawn potassium doped W fibers with about 2.4 mm length and 0.15 mm diameter were provided by Xiamen Honglu Tungsten and Molybdenum Industry Co., Ltd. The Y_2O_3 coating on the short W fibers was deposited by Physical Vapor Deposition in a Prevac magnetron sputtering system. The Y_2O_3 coating was prepared under the metallic mode according to Ref. [9]. The magnetron target material was pure Y metal (Kurt J. Lesker Company, 99.9% purity, 76.2 mm diameter, 6.35 mm thickness). The distance between the target and the substrate is about 15 cm. Argon was used to generate the plasma. Oxygen was injected as the reactive gas. The Ar flow rate was constant at 25 sccm in all cases. The vacuum chamber background pressure was about 5×10^{-8} mbar and the pressure during deposition was about 6.5×10^{-3} mbar. The thickness of the Y_2O_3 coating after deposition was about 1.6 μm.

2.2. The fabrication of the W_f/W composites

The short W fibers with a volume fraction of 40% and the W powders with different particle size (Xiamen Honglu Tungsten and Molybdenum Industry Co., Ltd) were mixed in a vessel for 24 h. The particle size of the W powder is 2 μm, 5 μm and 10 μm. The mixture was then put in a graphite mold with a diameter of 30 mm. Pure molybdenum foils with a thickness of 25 μm were added between the compressed sample and the graphite mold to reduce the carbon contamination during the sintering process. The W_f/W composites were sintered via field assisted sintering technology in a spark plasma sintering (SPS) furnace (SINTERLAND, LABOX-350). The sample was heated at a constant rate of 200 °C/min in a vacuum with a pressure below 0.1 mbar. The sintering temperature was set to 1600 °C and the holding time is 5 min. A constant pressure of 40 MPa was maintained throughout the sintering process.

2.3. The microstructural characterization

A scanning electron microscope (SEM) Zeiss GeminiSEM 300 was used to investigate the microstructure of Y_2O_3 coating and W_f/W composites. The electron backscatter diffraction (EBSD) analysis was conducted by a TESCAN MIRA3 SEM equipped by HKL Channel 5 software and an Oxford AZtec EBSD probe. In order to acquire EBSD maps with high quality, the samples for EBSD investigation were polished by diamond polishing liquid, and then plasma polished by an Argon ion polisher (Gatan Inc. 697. C). X-ray diffraction (XRD) was performed by an X-ray goniometer of the type Bruker Discover 8 with a solid copper target. The samples for XRD analysis were compressed bulk specimens composed by W powder and coated W fiber. The samples for transmission electron microscope (TEM) investigation were prepared by

Table 1
The properties of the W matrix, W fiber and FCC-Y_2O_3 for FEA modelling.

	W matrix	W fiber	FCC-Y_2O_3	Temperature (°C)
Elastic modulus (GPa)	400 [11]	400 [11]	170 [12]	25
	347 [13]	347 [13]	75 [12]	1400
	341 [13]	341 [13]	50	1500
	335 [13]	335 [13]	25 [12]	1600
Poisson's ratio	0.28 [13]	0.28 [13]	0.3 [11]	25–1600
Ultimate strength (MPa)	380 [11]	1968	1100 [12]	25
	300	400	283 [12]	1400
	200	300	193	1500
	150	200	103 [12]	1600
Yield strength (MPa)	–	1500 [14]	800 [12]	25
	250	350	226 [12]	1400
	150	250	154	1500
	100	150	83 [12]	1600

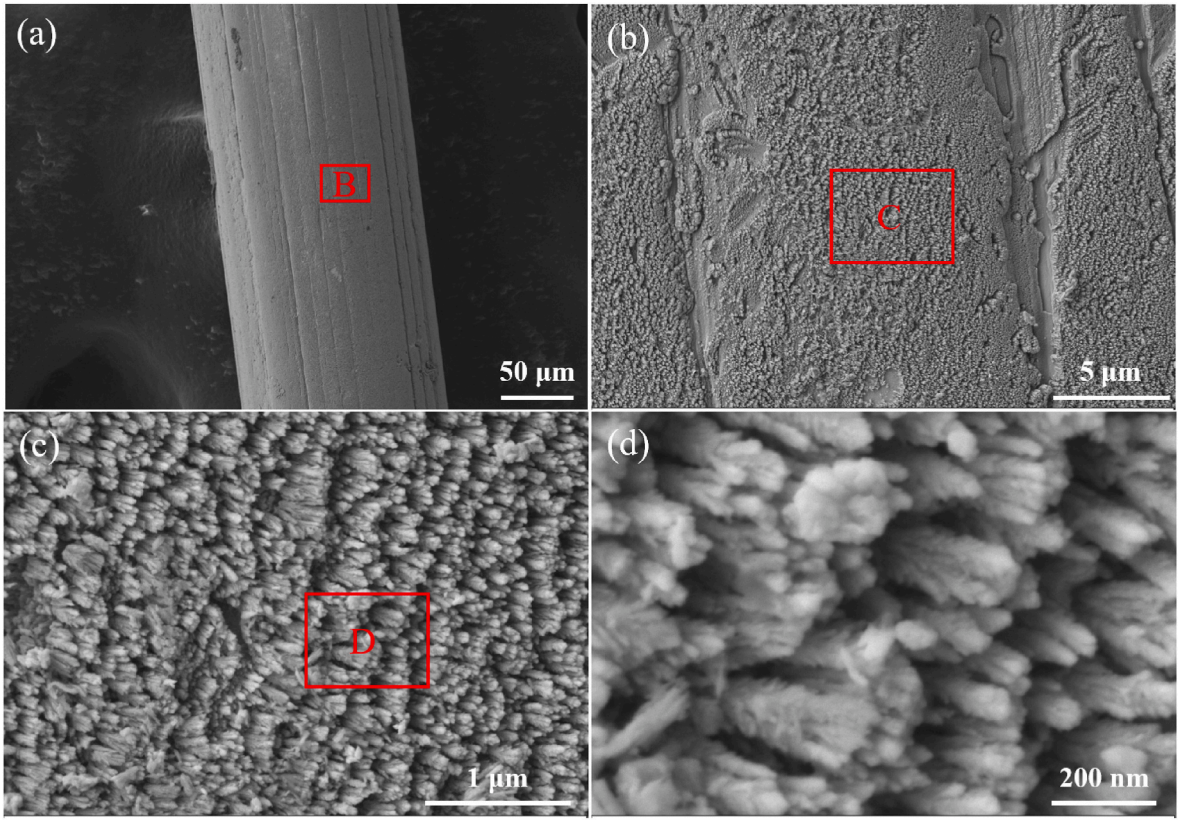

Fig. 2. The microstructure of the Y_2O_3 coating on the W fiber. (a) The surface of Y_2O_3 coating on the W fiber. (b) The enlarged region B in figure (a). (c) The enlarged region C of figure (b). (d) The enlarged region D of figure (c).

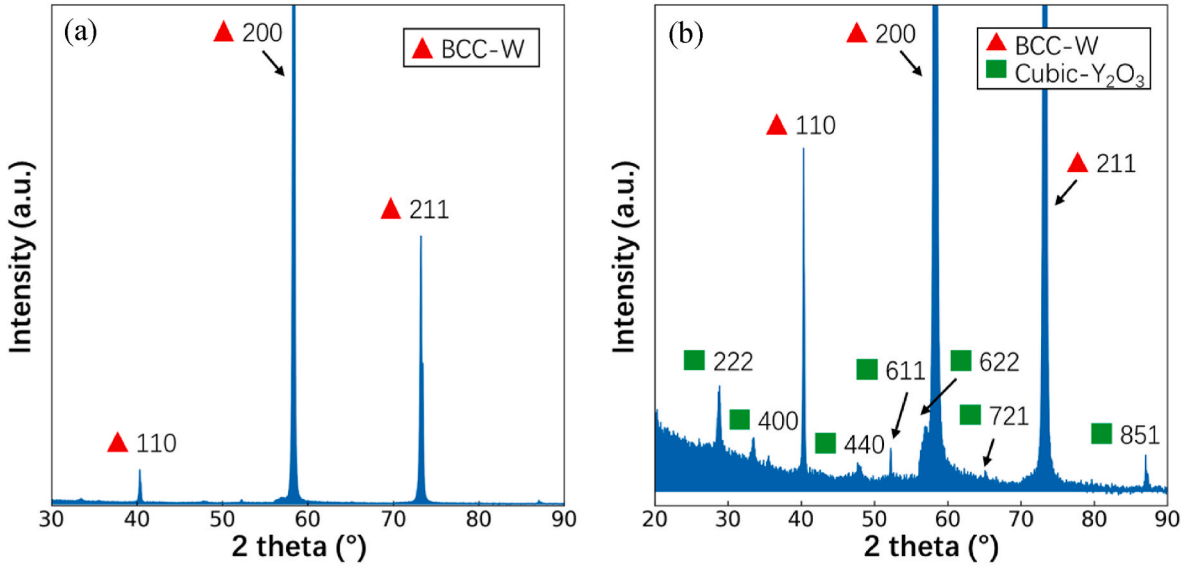

Fig. 3. XRD patterns of the tungsten fibers coated by Y_2O_3. (a) The overall patterns. (b) The detailed patterns at the relatively low intensity region.

focused ion beam (FIB) conducted on a Helios NanoLab G3 UC SEM. The TEM observation was conducted with a Tecnai G2 F20 S-TWIN transmission electron microscope and the operated accelerating voltage is 200 kV. The high-resolution TEM (HRTEM) was conducted on Titan G2 60–300 with image corrector.

2.4. Finite element model (FEM)

The FEM was performed using the commercial software ABAQUS Standard 2021. The simplified 3D model was constructed to reduce the computational effort, as shown in Fig. 1. The W fibers were homogenized to a continuous layer which had a planar surface to the surrounding W matrix and Y_2O_3 interface. The W powder is set as hemisphere to facilitate the application of pressure. The interface between W fiber, Y_2O_3 coating and W matrix is modelled by a cohesive contact. The detailed parameters were shown in section 4.2. The input parameters of W matrix, W fibers and Y_2O_3 coating used for modelling are shown in Table 1. The modelling results show the distribution of von

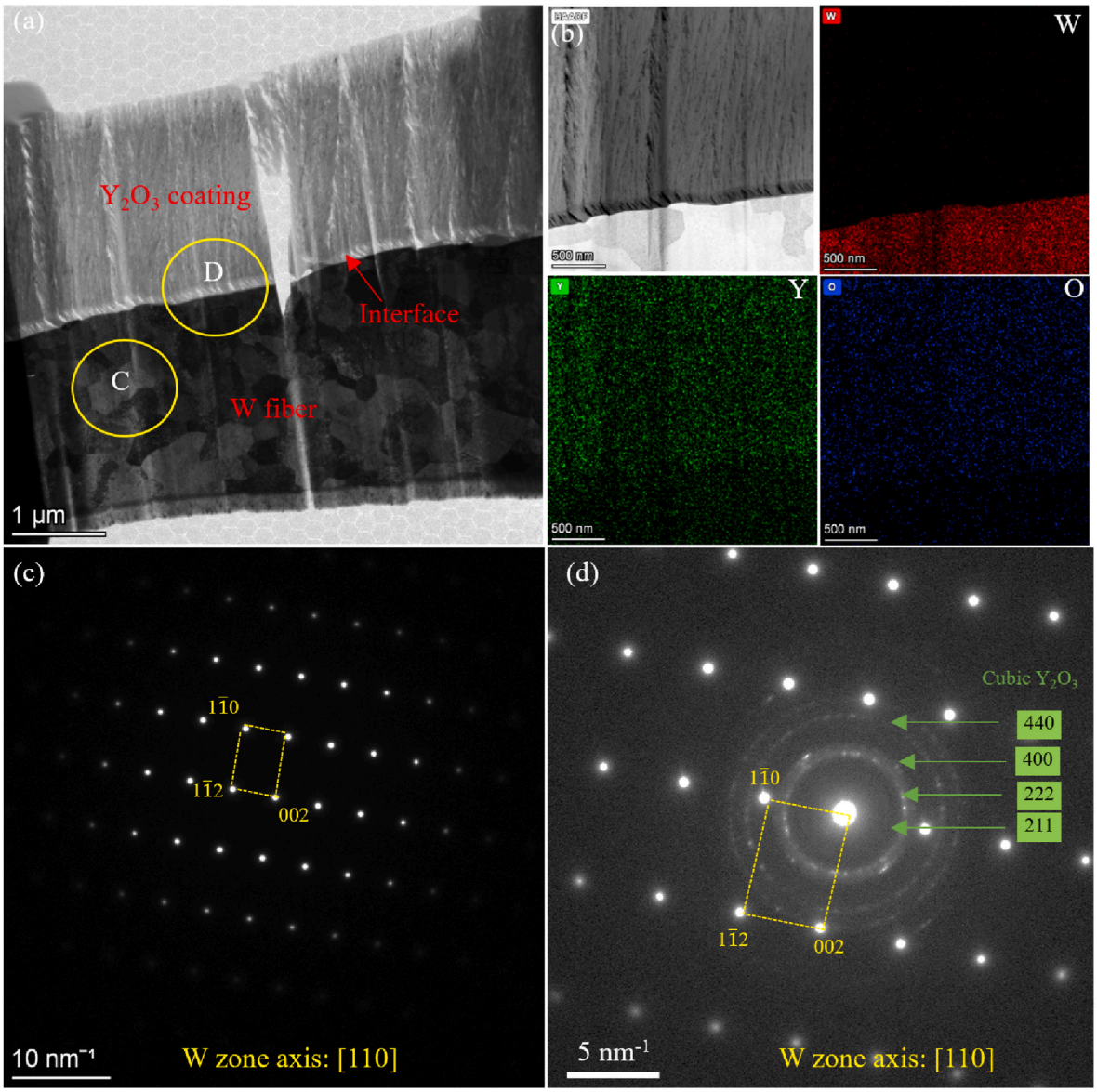

Fig. 4. (a) The microstructure of W fibers and the Y_2O_3 coating at the interface. (b) High-angle annular dark field (HAADF) images and the distribution of W, Y, and O elements at the interface. (c) The corresponding selected area diffraction patterns (SADPs) of region C in the W fiber of figure (a). (d) The corresponding SADPs of region D at the interface in figure (a).

Mises stress in the W_f/W composites, which is used for analyzing the failure behavior of Y_2O_3 coating during sintering.

3. Results

3.1. The microstructure of the Y_2O_3 coating on the W fiber

Fig. 2 shows the microstructure of the Y_2O_3 coating deposited on the surface of short W fibers before the sintering process. As shown in Fig. 2a and b, parallel lines can be seen on the surface of the fibers due to the drawing process. The Y_2O_3 coating is intact and dense, which is composed of nano-pillars on the coating surface, as shown in Fig. 2c and d. The diameter of the nano-pillars is about 20 nm.

The phases of the W fibers with Y_2O_3 coating are investigated by XRD, as shown in Fig. 3. The W fibers show body centered cubic (BCC) crystal structure with very high intensity, as shown in Fig. 3a. Although the diffraction intensity of Y_2O_3 is much lower than that of W, the diffraction peaks of Y_2O_3 can be clearly seen in Fig. 3b. The Y_2O_3 coating is the cubic (Ia-3) phase, which is similar with the Y_2O_3 coating deposited on Si [15]. The microstructure of the Y_2O_3 coating on the W fiber was further investigated by TEM, as shown in Fig. 4. In Fig. 4a, a set of nano-size Y_2O_3 columns was observed in the coating. Meanwhile, nano-sized grains or subgrains with high density of dislocations can be seen in the as-drawn W fibers. The average grain size is about 250 nm. In Fig. 4a, the zone C shows the region in W fiber. The zone D shows the region at the interface composed of W fiber and Y_2O_3 coating. The selected area diffraction patterns (SADPs) in region C of W fiber shows the crystal zone axis is $[110]_W$. The corresponding SADPs at the interface region D of Fig. 4a is shown in Fig. 4d. Both the diffraction spots of the W matrix and diffraction rings of polycrystalline Y_2O_3 are presented. The diffraction rings also show that the cubic phase is developed in Y_2O_3 coating, which is consistent with the result of XRD. The lattice parameter of cubic-Y_2O_3 is calculated to be 1.07 nm.

3.2. The interfacial microstructure in the W_f/W composites after sintering

The microstructure of the W_f/W composites sintered at 1600 °C is shown in Fig. 5. A layer of Y_2O_3 is visible at the interface between the W

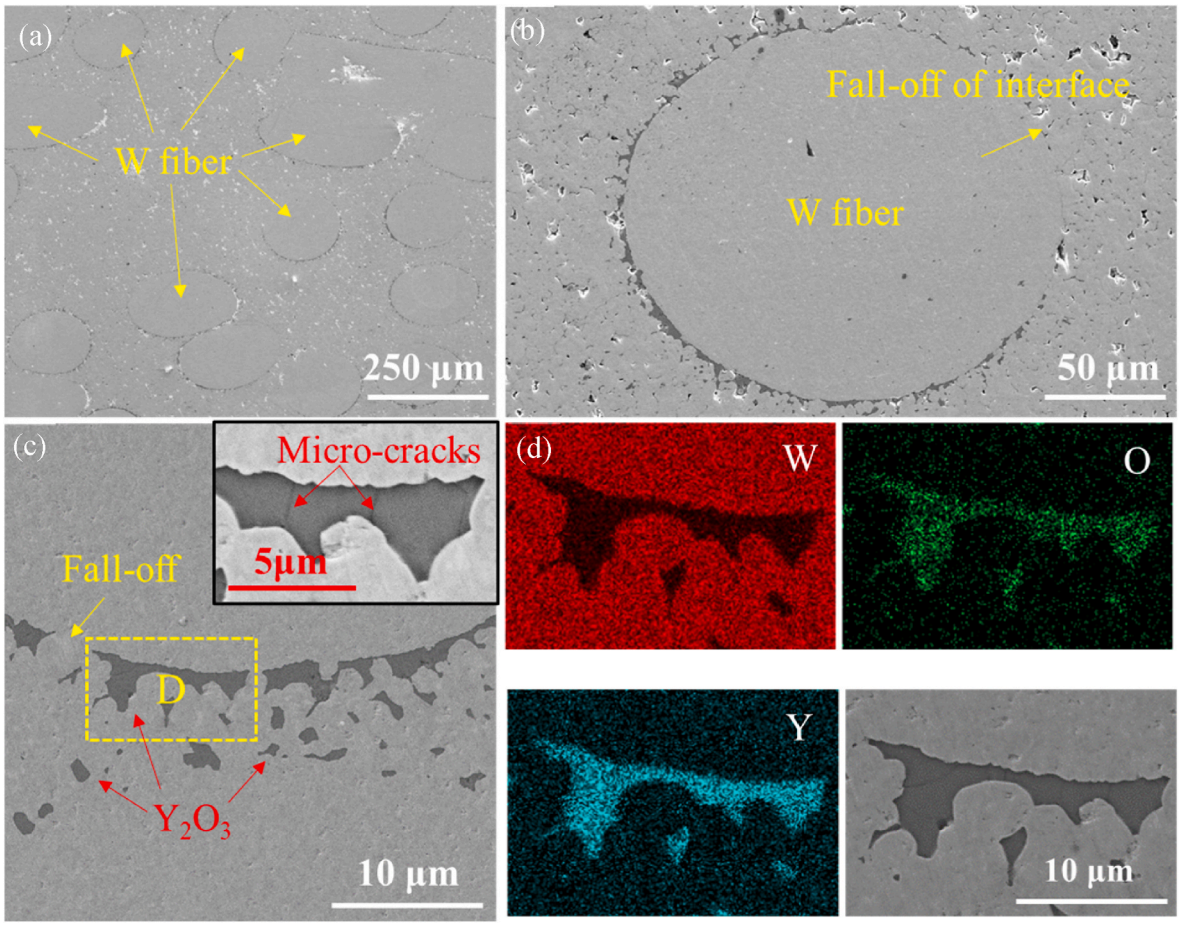

Fig. 5. Microstructure of the W_f/W composites sintered at 1600 °C. (a) SEM image of the W fiber and Y_2O_3 coating in the W_f/W composites. (b, c) The morphology of Y_2O_3 coating on the W fiber at the interface. (d) Distribution of W, Y and O at the interface between W fiber and W matrix in the region D of figure (c).

fibers and W matrix. However, the morphology of the Y_2O_3 interface is inhomogeneous and discontinuous. Some region of these W fibers has no Y_2O_3 interface, where the fiber and W powder are directly bonded together, as shown in Fig. 5b. It means that the Y_2O_3 interface falls off during sintering. Meanwhile, the Y_2O_3 interface contains many microcracks (Fig. 5c). The fractured Y_2O_3 interface breaks away from the W fiber surface, resulting in distribution of many large Y_2O_3 particles in the W matrix, as shown in Fig. 5c and d. The size of these large Y_2O_3 particles can reach several micrometers, which may deteriorate the mechanical property of the W_f/W composites.

The microstructure of the W_f/W composites were also investigated by EBSD maps, as shown in Fig. 6. In Fig. 6a and b, the Y_2O_3 phase shows brighter than the W phase in the image quality map, as indicated by arrows. The Y_2O_3 is indexed correctly by the EBSD patterns to have face centered cubic (FCC) crystal structure, as shown in Fig. 6c. Compared with Fig. 6c and d, it can be seen that the grains in the Y_2O_3 interface with different orientations are developed. The grain size of these Y_2O_3 can reach several micrometers, which is different from that of the original deposited Y_2O_3 coating in Fig. 4. For the microstructure of W fiber, it still shows fine grains with a grain size of about 500 nm.

The fractured Y_2O_3 interface and particles are further investigated by TEM, as shown in Fig. 7. Fig. 7a shows the Y_2O_3 interface between the W fiber and W matrix in the W_f/W composites. The microcracks are also observed in the Y_2O_3 interface, which is consistent with the SEM results. Meanwhile, the microcracks at the interface between W fiber and Y_2O_3 are also developed. Fig. 7b shows a Y_2O_3 particle with the shape of triangle in the W matrix. According to the SADPs of this Y_2O_3 particle, the crystal structure of Y_2O_3 is changed from cubic to FCC after sintering. The microstructure of FCC-Y_2O_3 particle has also been investigated by High Resolution Transmission Electron Microscope (HRTEM), as shown in Fig. 7c. The corresponding fast Fourier transform (FFT) images of Fig. 7c show the presence of faint superlattice reflections and secondary diffraction in Fig. 7d. The crystal zone axis is $[11\bar{2}]_{Y_2O_3}$. The lattice parameter of the FCC-Y_2O_3 is calculated to be 0.536 nm.

4. Discussions

4.1. The facture mechanism of Y_2O_3 interface in W_f/W composites

It has been found that the fracture of Y_2O_3 interface is bad for the toughness of W_f/W composites [4,8–10]. Three main reasons should be taken into consideration attributed to the fracture of the Y_2O_3 interface. Firstly, it is the phase transformation of the Y_2O_3 interface during sintering. In this study, the Y_2O_3 coating before sintering is cubic crystal structure. The lattice parameter of cubic-Y_2O_3 is about 1.07 nm. However, the cubic phase of Y_2O_3 changes to FCC-Y_2O_3 after sintering. The lattice parameter of the FCC-Y_2O_3 is about 0.536 nm, which is half of that of cubic Y_2O_3. It means that the volume of the Y_2O_3 coating changes induced by phase transformation after sintering, which may result in the fracture of the Y_2O_3 coating. The typical interfacial microstructure between the W fiber and FCC-Y_2O_3 is shown in Fig. 8. The space distance of $\{310\}_W$ is about 0.100 nm, and the space distance of $\{220\}_{Y_2O_3}$ is 0.196 nm. The lattice misfit between these two planes is up to 49.0%. It means that the interfacial energy is very high and not stable.

The second reason for the failure of the Y_2O_3 interface may be the large difference in the elastic modulus and thermal expansion coefficient between W and Y_2O_3. The elastic modulus of the FCC-Y_2O_3 at room

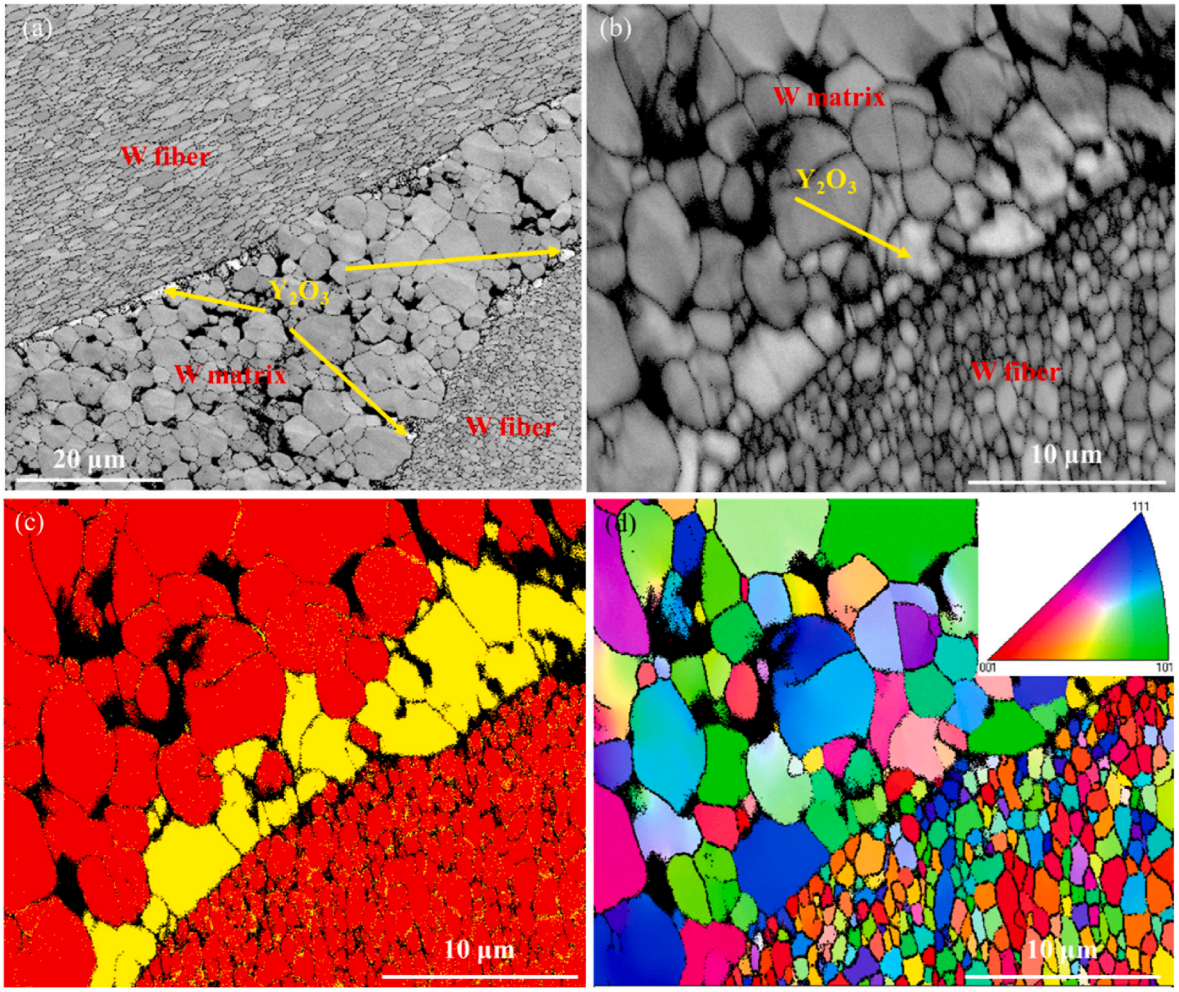

Fig. 6. (a) Microstructure of the W_f/W composites investigated by EBSD image quality map. (b) Image quality map, the corresponding (c) phase map and (d) orientation map showing the microstructure at the interface. In the phase map of Fig. c, the red color shows the W phase, and the yellow color shows the Y_2O_3 phase with FCC crystal structure. The step size is 50 nm. (For interpretation of the references to color in this figure legend, the reader is referred to the Web version of this article.)

temperature is about 150 GPa [12]. However, the elastic modulus of W fibers is about 406 GPa [16]. It means that large modulus misfit exists at the interface. Meanwhile, the thermal expansion coefficient of W at 1900K is about 18.37 × 10^{-6}/K [17], which is significantly different from that of Y_2O_3 (about 4.30 × 10^{-5}/K at 1900K) [18]. Therefore, large thermal stress (about 7000 MPa) appears at the interface during sintering at 1600 °C, which is much larger than the interfacial shear strength investigated by push-out tests (447 MPa) [19].

Finally, the fracture of the Y_2O_3 interface can also result from the hot compression due to the load of W particles on the Y_2O_3 interface during sintering. As shown in Fig. 5c, many W powders are pushed into the Y_2O_3 interface. During the sintering process, a pressure of 40 MPa was added to the samples. The stress distribution was analyzed by FEM, as shown in Fig. 9a. A very large stress of 1833 MPa is loaded on the W fiber, which is much higher than that of the yield strength (about 83 MPa [12]) and the ultimate compressive strength of the FCC-Y_2O_3 coating (about 103 MPa [12]). Therefore, the Y_2O_3 interface will be compressed to be plastic deformation and fracture during sintering. This large stress can also be reflected from the pores on the surface of W fiber, as shown in Fig. 9b.

4.2. *The effect of sintering process parameters on the interfacial microstructure*

The Y_2O_3 interface is essential in improvement of the fracture toughness of the W_f/W composites, due to weakening the interfacial adhesion energy between the W fiber and matrix, simultaneously impeding the abnormal recrystallization and grain growth of W fibers, which make the W fiber brittle [8–10]. However, the fracture of the Y_2O_3 coating on the W fiber usually occurs during the sintering process. Besides, the Y_2O_3 coating drops off from the W fiber and is scattered into W matrix. The fractured Y_2O_3 interface was dispersed as large particles in the W matrix, which may act as the fracture source in the W_f/W composites [4]. Thus, it is virtual to keep the integrity of Y_2O_3 interface during the sintering of the W_f/W composites. Therefore, the fracture behavior of the Y_2O_3 interface during sintering was studied by FEM, as shown in Fig. 10. The properties of W matrix, W fibers and FCC-Y_2O_3 were selected based on previous studies and summarized in Table 1 [12, 11,13,14]. The median value is utilized for modeling in the absence of previous research. The grey color in these figures means that the fracture of Y_2O_3 interface occurs. It can be seen that the failure of Y_2O_3 interface is closely related with the process parameters of the W_f/W composites, such as the sintering temperature, the pressure, the particle size of W powder and the thickness of Y_2O_3 interface. Higher sintering temperature and pressure are beneficial for the densification of W matrix, but

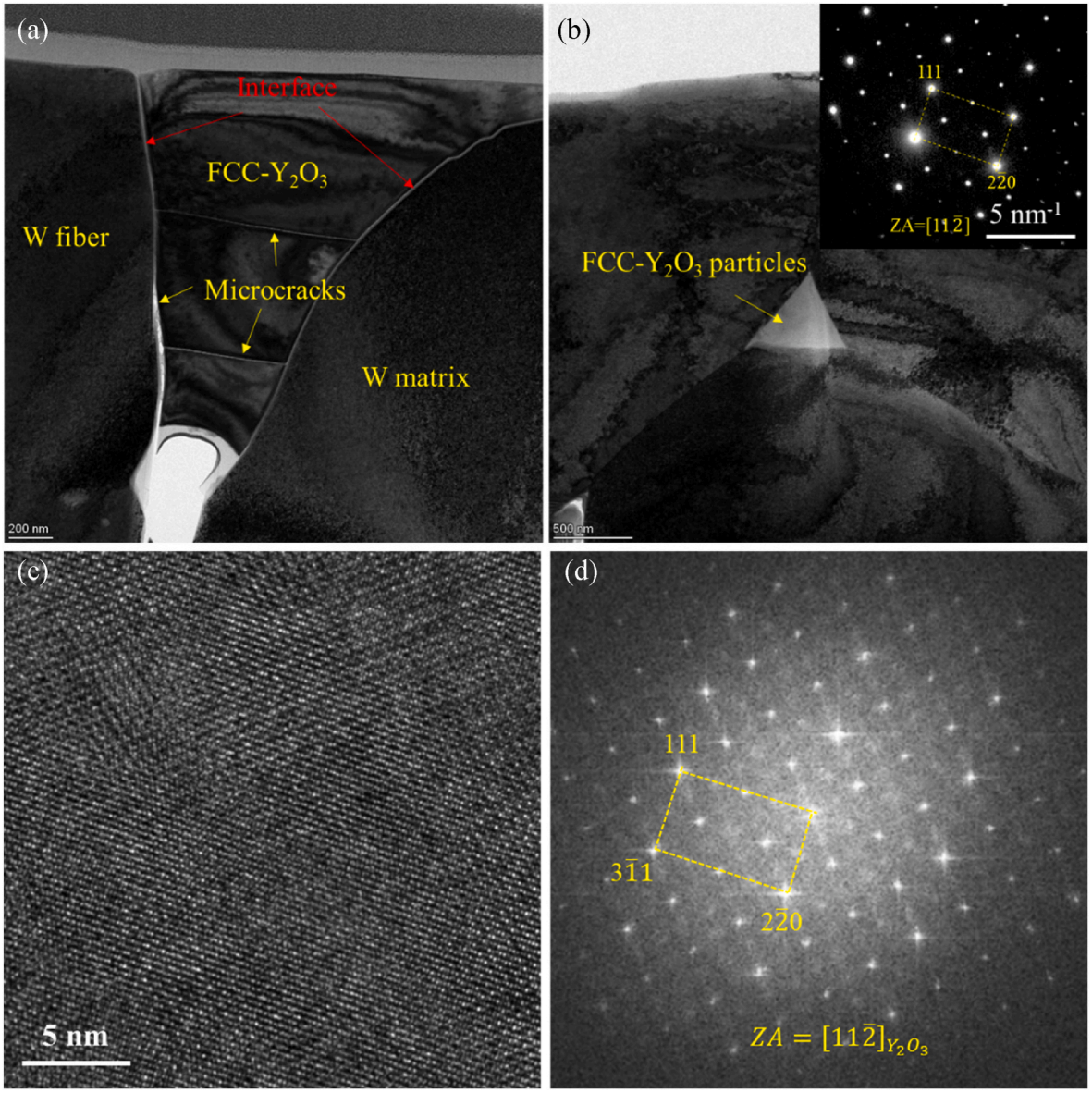

Fig. 7. (a) TEM image showing the microcracks in the Y_2O_3 interface between W fiber and W matrix. (b) TEM image showing the fractured Y_2O_3 particle in the W matrix. The inserted SADPs are obtained from the fractured Y_2O_3 particle. (c) HRTEM and (d) corresponding FFT images investigated the Y_2O_3 particle along [11 $\bar{2}$] crystal zone axis.

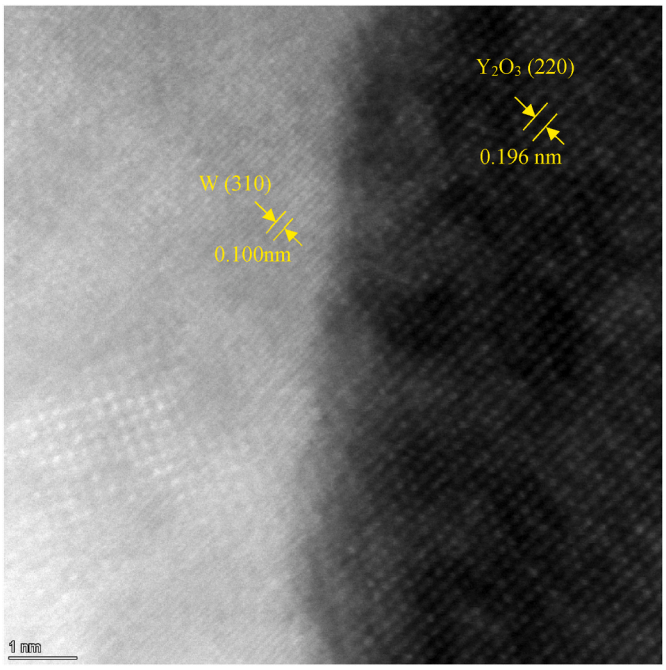

Fig. 8. The interface microstructure between FCC-Y_2O_3 and W in the W_f/W composites.

easily inducing the fracture of the Y_2O_3 interface. Meanwhile, larger particle size of W powder and thinner Y_2O_3 interface are beneficial for the fracture of Y_2O_3 interface. It has been found that the Y_2O_3 interface with a thickness of 2.5 μm is more complete than that of the Y_2O_3 interface with a thickness of 1.0 μm in the W_f/W composites after sintering [9]. For the W_f/W composites with a sintering temperature of 1600 °C, particle size of 5 μm, pressure of 40 MPa, the thickness of the Y_2O_3 coating should be thicker than 1.6 μm to prevent the fracture of Y_2O_3 interface, as shown in Fig. 10a, b and c. In Fig. 10d, e and f, for the W_f/W composites with a sintering temperature of 1600 °C, particle size of 5 μm, Y_2O_3 interface with a thickness of 1 μm, the added pressure should be lower than 20 MPa. For the W_f/W composites with a sintering temperature of 1600 °C, pressure of 40 MPa, Y_2O_3 interface with a thickness of 1 μm, the particle size of W powder should be smaller than 2 μm, as shown in Fig. 10g, h and i.

It can be concluded from the simulation results, in order to obtain high relative density for the W_f/W composites, the higher sintering temperature and pressure are usually needed. In that condition, the particle size of W powder should be smaller and the thickness of Y_2O_3 interface should be thicker. Based on the results of FEM, in order to restrict the fracture of Y_2O_3 interface, if the pressure is 40 MPa, the particle size of W powder is 5 μm and the thickness of Y_2O_3 interface is 1.6 μm, the sintering temperature should be selected to be lower than 1600 °C. Under this condition, the experimental result of the W_f/W composites prepared at 1600 °C is shown in Fig. 11. Although microcracks can be seen in the Y_2O_3 interface, the Y_2O_3 interface can be maintained on the W fiber in the W_f/W composites. According to the previous study, when the sintering temperature reached 1800 °C under similar conditions, the Y_2O_3 interface was broken and dispersed into the W matrix during sintering, resulting in the limitation of debonding between W fiber and matrix [8]. Therefore, the selection of appropriate processing parameters is very important for the preparation of W_f/W composites with complete Y_2O_3 interface structure.

5. Conclusions

In this study, the interfacial microstructure in the discontinuous short W_f/W composites with Y_2O_3 coating on the W fiber was investigated. Meanwhile, the fracture behavior of the Y_2O_3 interface was investigated by both the experiments and FEA. The main conclusions are drawn as follow.

(1) The crystal structure of Y_2O_3 coating is cubic, and it changes to be face centered cubic after sintering. The lattice parameter of cubic-Y_2O_3 is about 1.07 nm, while the lattice parameter of the FCC-Y_2O_3 is about 0.536 nm.
(2) After sintering, microcracks are usually observed in the Y_2O_3 interface. Meanwhile, the fractured Y_2O_3 interface falls off from the W fiber and is scattered into W matrix as large Y_2O_3 particles with a size of several micrometers.
(3) The reasons for the fracture of the Y_2O_3 interface can be attributed to the large lattice misfit at the interface, and the large difference in the elastic modulus and thermal expansion coefficient between W and FCC-Y_2O_3.
(4) The failure behavior of the Y_2O_3 interface was investigated through FEM considering the processing parameters of the sintering temperature, the pressure, the particle size of W powders and the thickness of Y_2O_3 coating. If the pressure is 40 MPa, the particle size of W powder is 5 μm and the thickness of Y_2O_3 interface is 1.6 μm, the sintering temperature should be selected to be lower than 1600 °C. The FEM results are consistent with the experimental results.

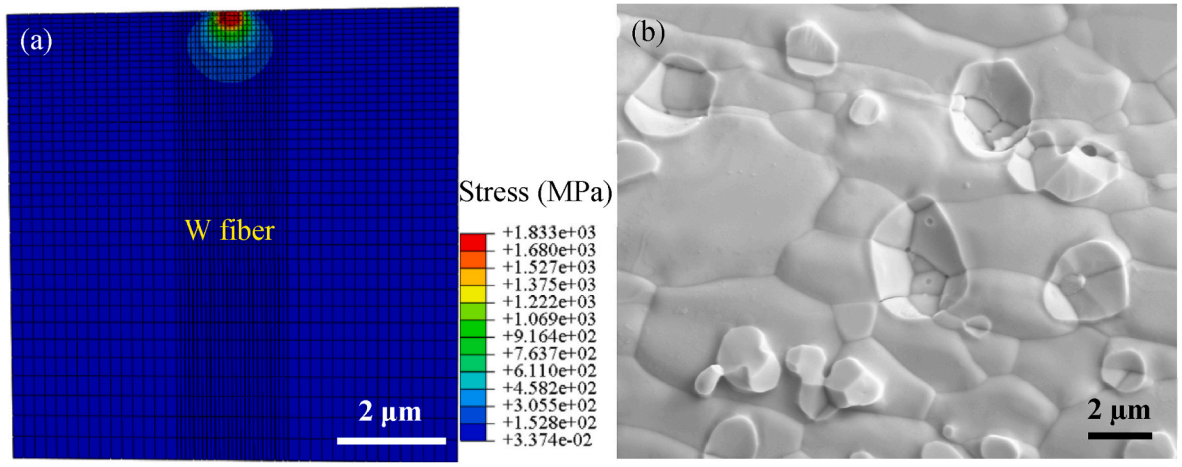

Fig. 9. (a) Distribution of von Mises stress in the W_f/W composites without the Y_2O_3 interface prepared by W powder with particle size of 5 μm. (b) The pores on the surface of W fiber compressed by W powder in the W_f/W composites.

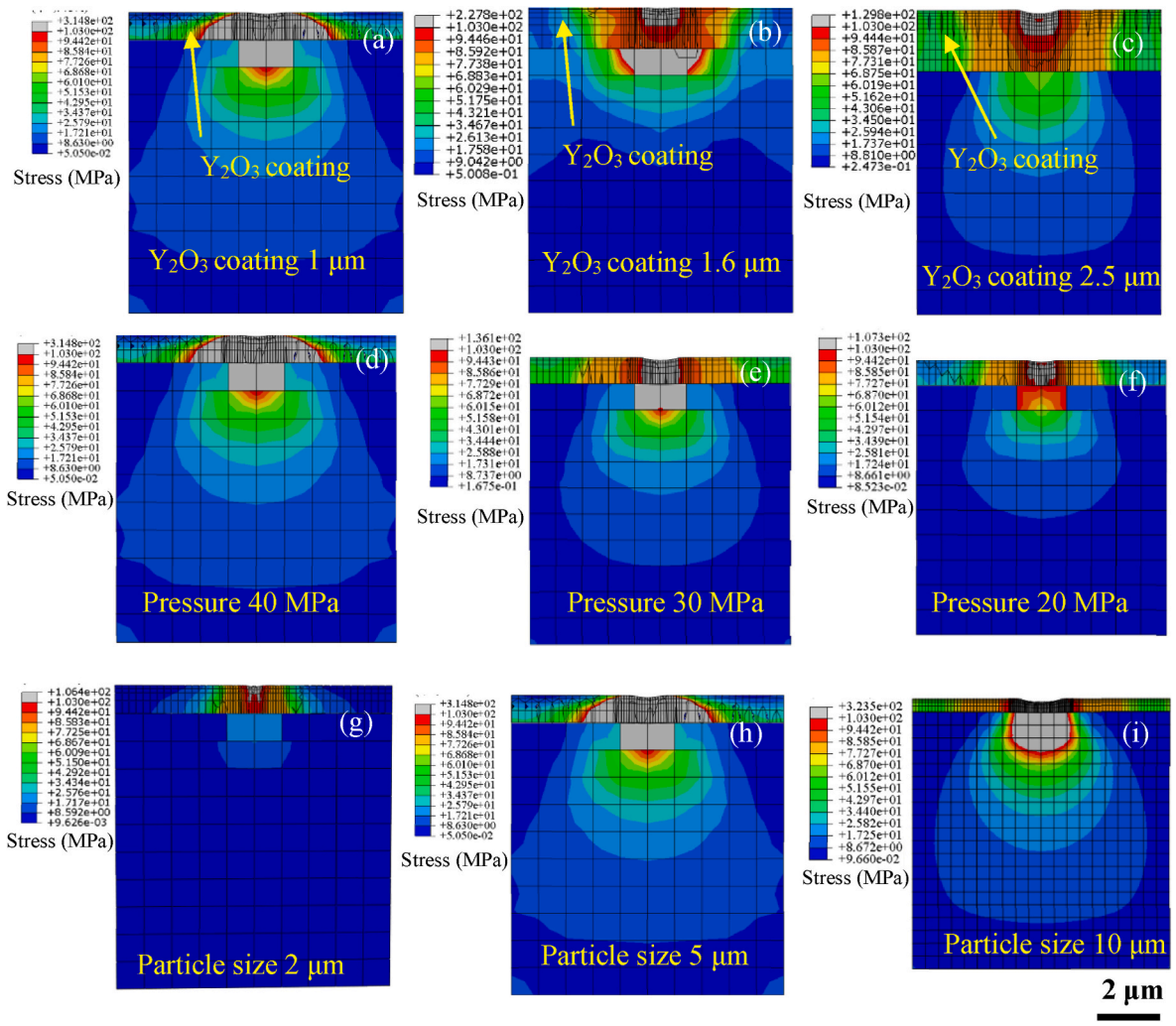

Fig. 10. The FEA results showing the stress distribution in the W_f/W composites with Y_2O_3 interface considering the sintering temperature, the pressure, the particle size of W powder and the thickness of Y_2O_3 interface. The W_f/W composites with a sintering temperature of 1600 °C, particle size of 5 μm, pressure of 40 MPa, and the thickness of Y_2O_3 interface (a) 1 μm, (b) 1.6 μm, (c) 2.5 μm. The W_f/W composites with a sintering temperature of 1600 °C, particle size of 5 μm, Y_2O_3 interface with a thickness of 1 μm, and the different pressure of (d) 40 MPa, (e) 30 MPa, (f) 20 MPa. The W_f/W composites with a sintering temperature of 1600 °C , pressure of 40 MPa, Y_2O_3 interface with a thickness 1 μm, and W powder with the particle size of (g) 2 μm, (h) 5 μm, (i) 10 μm.

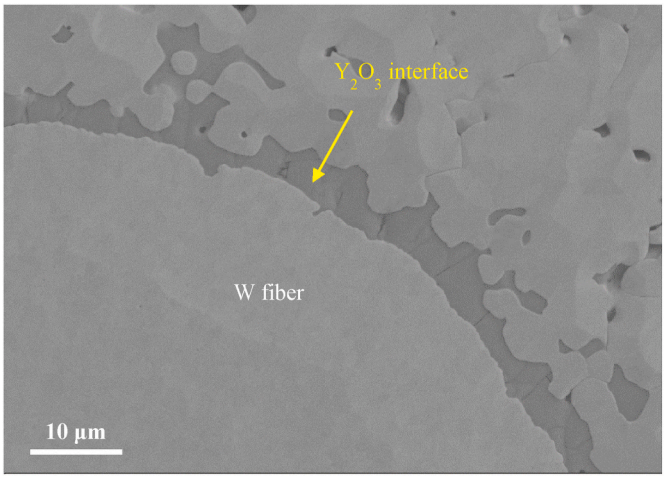

Fig. 11. The interfacial microstructure of W_f/W composites sintered at 1500 °C. The particle size of W powder is 5 μm, the pressure is 40 MPa, a thickness of Y_2O_3 interface is 1.6 μm.

Data availability statement

The raw data related to this manuscript would be made available on request.

Declaration of competing interest

The authors declare that they have no known competing financial interests or personal relationships that could have appeared to influence the work reported in this paper.

Acknowledgments

This work is supported by the International Cooperation Fund of Anhui Province (202104b11020023), Natural Science Foundation of Anhui Province (2308085ME134), National Natural Science Foundation of China (12205070), the Fundamental Research Funds for the Central Universities (PA2023GDSK0056, PA2023GDGP0042).

References

[1] Butler BG, Paramore JD, Ligda JP, Ren C, Fang ZZ, Middlemas SC, Hemker KJ. Mechanisms of deformation and ductility in tungsten - a review. Int J Refract

Metals Hard Mater 2018;75:248–61. https://doi.org/10.1016/j.ijrmhm.2018.04.021.
[2] Neu R, Riesch J, Coenen JW, Brinkmann J, Calvo A, Elgeti S, García-Rosales C, Greuner H, Hoeschen T, Holzner G, Klein F, Koch F, Linsmeier Ch, Litnovsky A, Wegener T, Wurster S, You J-H. Advanced tungsten materials for plasma-facing components of DEMO and fusion power plants. Fusion Eng Des 2016;109–111:1046–52. https://doi.org/10.1016/j.fusengdes.2016.01.027.
[3] Du J, Höschen T, Rasinski M, You J-H. Shear debonding behavior of a carbon-coated interface in a tungsten fiber-reinforced tungsten matrix composite. J Nucl Mater 2011;417:472–6. https://doi.org/10.1016/j.jnucmat.2010.12.254.
[4] Mao Y, Coenen JW, Riesch J, Sistla S, Almanstötter J, Jasper B, Terra A, Höschen T, Gietl H, Linsmeier Ch, Broeckmann C. Influence of the interface strength on the mechanical properties of discontinuous tungsten fiber-reinforced tungsten composites produced by field assisted sintering technology. Composites Part A 2018;107:342–53. https://doi.org/10.1016/j.compositesa.2018.01.022.
[5] Du J, Höschen T, Rasinski M, Wurster S, Grosinger W, You J-H. Feasibility study of a tungsten wire-reinforced tungsten matrix composite with ZrOx interfacial coatings. Compos Sci Technol 2010;70:1482–9. https://doi.org/10.1016/j.compscitech.2010.04.028.
[6] Du J, Höschen T, Rasinski M, You J-H. Interfacial fracture behavior of tungsten wire/tungsten matrix composites with copper-coated interfaces. Mater Sci Eng 2010;527:1623–9. https://doi.org/10.1016/j.msea.2009.10.046.
[7] Gietl H, Riesch J, Zielinski M, Höschen T, Coenen JW, Schönen S, Neu R. Interlayer properties of tungsten fibre-reinforced composites and their determination by different methods. Nuclear Materials and Energy 2021;28:101060. https://doi.org/10.1016/j.nme.2021.101060.
[8] Shu R, Mao Y, Coenen JW, Terra A, Liu C, Schönen S, Höschen T, Riesch J, Linsmeier C, Broeckmann C. Microstructure and mechanical properties of W_f/W composites influenced by Y_2O_3 coating. Int J Refract Metals Hard Mater 2023;115:106322. https://doi.org/10.1016/j.ijrmhm.2023.106322.
[9] Mao Y, Engels J, Houben A, Rasinski M, Steffens J, Terra A, Linsmeier Ch, Coenen JW. The influence of annealing on yttrium oxide thin film deposited by reactive magnetron sputtering: process and microstructure. Nuclear Materials and Energy 2017;10:1–8. https://doi.org/10.1016/j.nme.2016.12.031.
[10] Shu R, Mao Y, Lau A, Coenen JW, Lau A, Liu C, Riesch J, Linsmeier C, Broeckmann C. Effect of the heating rate and Y_2O_3 coating on the microstructure of W_f/Y_2O_3/W composites via field assisted sintering technology. Nuclear Materials and Energy 2024;38:101602. https://doi.org/10.1016/j.nme.2024.101602.
[11] Shu R, Mao Y, Coenen JW, Terra A, Liu C, SchÖnen S, Riesch J, Linsmeier C, Broeckmann C. Interface and mechanical properties of the single-layer long fiber reinforced W_f/W composites fabricated via field assisted sintering technology. Mater Sci Eng 2022;857:144098. https://doi.org/10.1016/j.msea.2022.144098.
[12] Özer Ü, Akinc M. Compressive properties of yttrium oxide. J Am Ceram Soc 1996;79:805–8. https://doi.org/10.1111/j.1151-2916.1996.tb07950.x.
[13] Lowrie R, Gonas AM. Single-crystal elastic properties of tungsten from 24° to 1800°C. J Appl Phys 1967;38:4505–9. https://doi.org/10.1063/1.1709158.
[14] Terentyeva D, Van Renterghem W, Tanure L, Dubinko A, Riesch J, Lebedieve S, Khvan T, Verbeken K, Coenen JW, Zhurkin EE. Correlation of microstructural and mechanical properties of K-doped tungsten fibers used as reinforcement of tungsten matrix for high temperature applications. Int J Refract Metals Hard Mater 2019;79:204–16. https://doi.org/10.1016/j.ijrmhm.2018.12.007.
[15] Gaboriaud RJ, Pailloux F, Guerin P, Paumier F. Yttrium sesquioxide, Y_2O_3, thin films deposited on Si by ion beam sputtering: microstructure and dielectric properties. Thin Solid Films 2001;400:106–10. https://doi.org/10.1016/S0040-6090(01)01468-7.
[16] Zhao P, Riesch J, Höschen T, Almanstötter J, Balden M, Coenen JW, Himml R, Pantleon W, von Toussaint U, Neu R. Microstructure, mechanical behaviour and fracture of pure tungsten wire after different heat treatments. Int J Refract Metals Hard Mater 2017;68:29–40. https://doi.org/10.1016/j.ijrmhm.2017.06.001.
[17] Bodryakov VY. Correlation of temperature dependences of thermal expansion and heat capacity of refractory metal up to the melting point: tungsten. High Temp 2015;53:643–8. https://doi.org/10.1134/S0018151X15040069.
[18] Şavklıyıldız İ. Thermal equation of state study of polymorphic phases of Y_2O_3. J Appl Phys 2021;129:085108. https://doi.org/10.1063/5.0043704.
[19] Gietl H, Riesch J, Zielinski M, Höschen T, Coenen JW, Schönen S, Neu R. Interlayer properties of tungsten fibre-reinforced composites and their determination by different methods. Nuclear Materials and Energy 2021;28:101060. https://doi.org/10.1016/j.nme.2021.101060.